

# Mechanical Meta-material of Multi-layered $\text{Al}_2\text{O}_3/\text{TiN}/\text{Al}_2\text{O}_3$ film as Large-surface Transmission Dynode

---

H.W. Chan,<sup>a,b,1</sup> V. Prodanović,<sup>a,b</sup> T. ten Bruggencate<sup>c</sup> C.W. Hagen,<sup>c</sup> P.M. Sarro,<sup>b</sup> and H. v.d Graaf<sup>a</sup>

<sup>a</sup>*National Institute for Subatomic Physics (NIKHEF),  
Science Park 105, 1098 XG, Amsterdam, The Netherlands*

<sup>b</sup>*Faculty of Electrical Engineering, Mathematics, and Computer science, Department of microelectronics/ECTM,  
Feldmannweg 17, 2628 CT, Delft, The Netherlands*

<sup>c</sup>*Faculty of applied sciences, Department of Imaging Physics, Delft University of Technology,  
Lorentzweg 1. 2628 CJ, Delft, The Netherlands*

E-mail: [h.w.chan@hotmail.com](mailto:h.w.chan@hotmail.com)

**ABSTRACT:** We present a novel manner in which to fabricate tri-layer transmission dynodes (tynodes). These tynodes are self-supporting and reinforced by silicon-oxide. This allows us to span a larger area, which is necessary for the development of the Timed Photon Counter. The performance of these tynodes is measured using a scanning electron microscope setup.

**KEYWORDS:** secondary electron emission; transmission dynode; photomultiplier; vacuum electron multipliers; atomic layer deposited alumina; ultra-thin films

ARXIV EPRINT: [1234.56789](https://arxiv.org/abs/1234.56789)

---

<sup>1</sup>Corresponding author.

---

## Contents

<b>1</b>	<b>Introduction</b>	<b>1</b>
<b>2</b>	<b>Design</b>	<b>4</b>
<b>3</b>	<b>Fabrication</b>	<b>6</b>
<b>4</b>	<b>Experimental setup</b>	<b>7</b>
4.1	Transmission secondary electron yield	7
4.2	Surface scan & Yield maps	8
<b>5</b>	<b>Results &amp; discussion</b>	<b>9</b>
5.1	Fabrication	9
5.2	Transmission secondary electron yield	9
5.3	Active surface & Collection efficiency	11
<b>6</b>	<b>Conclusion &amp; Outlook</b>	<b>14</b>
<b>A</b>	<b>Secondary electron yield map</b>	<b>15</b>

---

## 1 Introduction

The Timed Photon Counter (TiPC) is a novel vacuum electron multiplier that has ultra-thin transmission dynodes (tynodes) as multiplication stages [1]. The detection principle is similar to a photomultiplier tube (PMT), namely photoemission from a photocathode and subsequent (secondary) electron multiplication in vacuum. In a PMT, a photoelectron is multiplied within a series of (reflective) dynodes [2]. The dynodes are carefully aligned in a sequence, where the electric potential is step-wisely increased between each dynode. Under influence of the electric field, the SEs are accelerated and directed from dynode to dynode. Their number increases until they reach the anode, which will provide an electrical signal as read-out. PMTs belong to one of the most sensitive photon detectors due to its high gain and low noise. However, there are some disadvantages due to the complex arrangement of the (reflective) dynodes. First, the non-uniform electron paths between each dynode limits the timing resolution to nanoseconds. Second, the electron paths are easily perturbed by external magnetic fields. And lastly, the device is large, fragile and expensive to manufacture.

TiPC will improve upon PMTs in terms of timing and spatial resolution by using tynodes. A tynode is an ultra-thin membrane that allows for transmission secondary electron emission (TSEE): an incoming primary electron (PE) will generate multiple transmission secondary electrons (TSE) within a membrane as the PE transmits through it. This allows tynodes to be closely stacked on top of each other, which benefits the timing resolution. The more homogenous and stronger electric

field between the tynodes will reduce the spread in arrival time of TSEs. Also, the TSEs are less susceptible to external magnetic field due to the increased electric field strength. Moreover, 2D spatial information can be acquired with the planar tynodes by using a CMOS pixelchip as read-out.

The performance of a tynode can be characterized by the maximum transmission yield  $\sigma_T^{\max}$  obtained with primary electron energy  $E_T^{\max}$ :  $\sigma_T^{\max}(E_T^{\max})$ . In a detector with multiple tynodes, the former will determine the overall gain, while the latter the required operating voltage. The required PE energy  $E_T^{\max}$  is correlated to the film thickness and the range of the electron in the film. After all, only SEs generated near the exit surface of the membrane has a chance to escape. As such, the thickness of the film is a parameter that needs to be optimized. In the past, several types of transmission dynodes with high transmission yields (TEY) have been reported [3]. Unfortunately, they were impractical due to the required PE energy to achieve it. For instance, a TEY of 27 (9 keV) was reported for a caesium-activated CsI film deposited on Al/Al<sub>2</sub>O<sub>3</sub> film by Hagino et al. [4]. A device with several of these tynodes will require a very large operating voltage.

Our group used Micro-Electro-Mechanical System (MEMS) technology to fabricate ultra-thin membranes, which were suspended within a supporting mesh with small circular windows with a diameter of 30  $\mu\text{m}$  [5]. The windows are arranged in a 64x64 array with a pitch of 55  $\mu\text{m}$  to match the spacing of the pixel pads on a TimePix chip. An aligned tynode stack will form a channel in which electron multiplication will take place and be read out by individual pixels as shown in figure 1. Two types of material was used to form the ultra-thin membrane: Low-pressure-chemical-vapor-deposition (LPCVD) silicon nitride and atomic-layer-deposition (ALD) aluminum oxide. The former has a transmission yield of 1.6 (2.8 keV) for a membrane with a thickness  $d = 40\text{ nm}$ , while the latter has a transmission yield of 2.6 (1.45 keV) for a membrane with  $d = 10\text{ nm}$ . On both tynode, a titanium nitride (TiN) layer is deposited on one side to provide in-plane conductivity. In a different process, the TiN layer was encapsulated within two layers of Al<sub>2</sub>O<sub>3</sub> to improve the

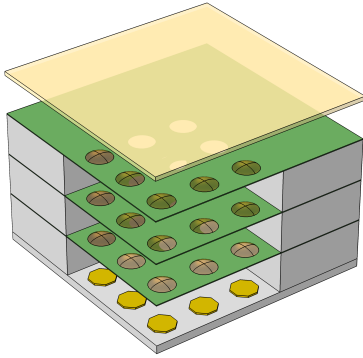


**Figure 1:** Schematic drawing of TiPC with tynodes comprised of a small window array

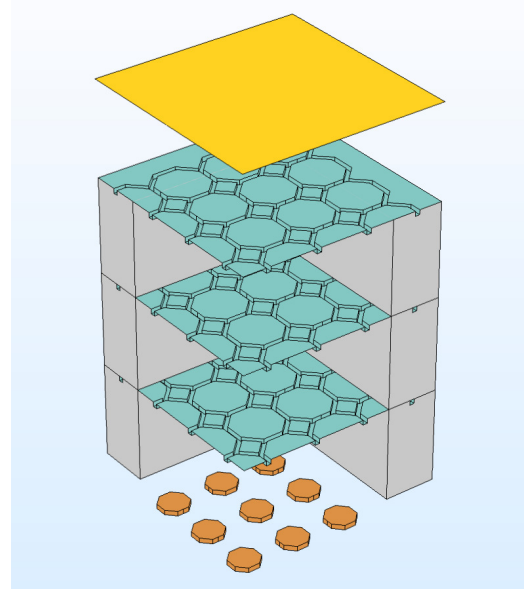


**Figure 2:** Schematic drawing of TiPC with metamaterial tynodes

reliability of the fabrication process [6]. This tri-layer film had a transmission yield of 3.1 (1.55 keV).

The supporting mesh is a necessity in the design of the tynode array due to the fragility of the ultra-thin films, but does not contribute to electron multiplication. Photoelectrons that are emitted from the photocathode above the mesh will not be detected. The collection efficiency of TiPC is therefore proportional to the active surface of the tynode, which can be estimated by the ratio between the surface of the small windows and the supporting mesh. For an array of windows with a diameter of 30  $\mu\text{m}$  and a displacement of 55  $\mu\text{m}$ , the active surface is only 23.4%. The collection efficiency is also dependent on successful electron multiplication within the tynode stack. Misalignment can potentially result in loss of SEs within the stack. A different concern is the accumulation of electrons within the dielectric material (SiN) of the mesh. During prolonged irradiation, charge can accumulate on the exposed surface of dielectric mesh and cause distortions in the electric field.

As such, new tynodes have been made with some improvements: increased window size, dome-shaped membranes, alignment grooves and a metal mesh cover [7]. First, the window diameter have been increased to 45  $\mu\text{m}$ , which improves the active surface to 52.6%. Second, the dome-shaped membranes have a focusing effect on SEs. SEs are directed to the center of the next dome and will stay within the 'channel' above the corresponding pixel pad. Third, alignment grooves are etched in the silicon frame of the tynode, which are used to place silicon dioxide spacers between each tynode. The alignment is expected to be within the accuracy of the photolithography process. And lastly, a metal layer covering the dielectric mesh will prevent PEs to be trapped. Also, the reliability of the conductive layer will improve, since the metal layer will be directly connected to the ultra-thin TiN layer. Although, these new features will address some of the concerns, it also increases the complexity of the fabrication process.

In this paper, we present an entirely different tynode design which eliminates the need of a supporting mesh by forming a mechanical meta-material. In a recent paper, ultra-thin mechanical metamaterial has been shown to exhibit enhanced flexibility, rigidity and strength in comparison with a flat membrane by Davani et al. [8]. They formed the metamaterial by depositing an ultra-thin ALD  $\text{Al}_2\text{O}_3$  film on a 3D honeycomb mold, which is removed afterwards by plasma etching. The improved properties are ascribed to the extruded (semi-open hollow) ribs which provide additional mechanical strength.

The metamaterial can be functionalized as a tynode by adding a conductive layer, such as titanium nitride, to the ALD  $\text{Al}_2\text{O}_3$  film [5, 6]. A tynode formed as a metamaterial has the same thickness continuously. Incoming electrons can generate SEs on any part of the structure. As a result, the effective area of these tynodes will be nearly 100% and the alignment precision in the tynode stack will be less stringent. In addition, the honeycomb-shaped domes will provide a focusing effect. Also, there is no longer a risk of any charge-up effect, since the thick dielectric mesh is no longer present. And lastly, the fabrication process is less complex in comparison. In figure 2, a schematic drawing of a TiPC detector with metamaterial tynodes have been drawn, which compared to figure 1 has a larger active surface for electron multiplication.

In this paper, metamaterials with two different patterns are presented: one with a hexagon/honeycomb pattern and one with an octagon pattern. The latter is designed to match the pitch of the pixel pads

of a TimePix chip. The secondary electron emission film is a tri-layer  $\text{Al}_2\text{O}_3/\text{TiN}/\text{Al}_2\text{O}_3$  film deposited by atomic-layer-deposition (ALD). The electron yield is determined with a collector-based method within a scanning electron microscope.

## 2 Design

Two periodic cellular patterns are considered in this paper: hexagonal/honeycomb and octagonal. The first is a hexagonal pattern similar to the one reported by Davami et al [8]. They have shown that metamaterials with this pattern have increased strength, flexural stiffness, rigidity and resistance to deformation. The free-standing plate material of alumina can have a length of up to 2 cm and are extremely light and resilient. Also, it has been demonstrated that it has shape-recovering properties. The bending stiffness is ascribed to the hexagon pattern in which any plane perpendicular to the plate is intersected by a vertical wall. In addition, any cracks have to propagate along the triangular lattice, which makes these materials more robust. They derived a design rule for new patterns: any plane perpendicular to the plate needs be intersected by a vertical wall.

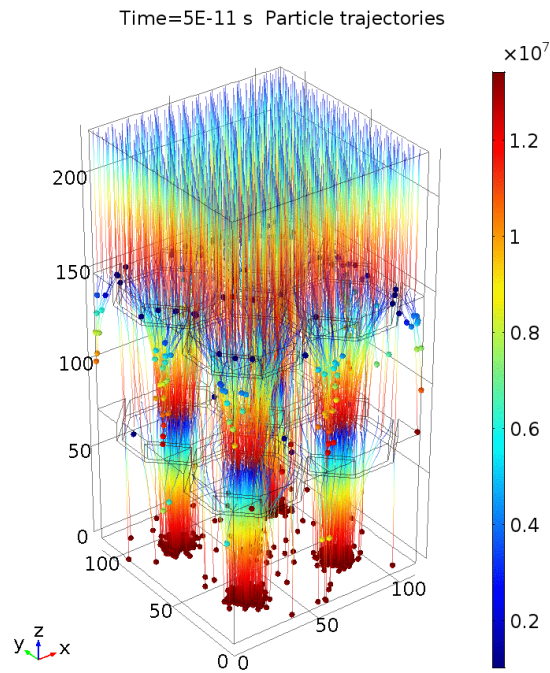


**Figure 3:** COMSOL simulation of a TiPC detector with two tynode stages. For the simulation, two modules of COMSOL was used: AC/DC and Charged Particle Tracing (CPT). The first module is used to simulate the static electric field.  $\Delta U = 1000 \text{ V}$  between each stage. The second module is used to simulate transmission secondary electron emission from the two tynode stages. Photoelectrons are released uniformly from the photocathode. Each incoming electron generates one transmission secondary electron on each tynode. Each PE and the SEs that they generate on each tynode will form a 'path'. This allow us to estimate the collection efficiency of a TiPC detector.

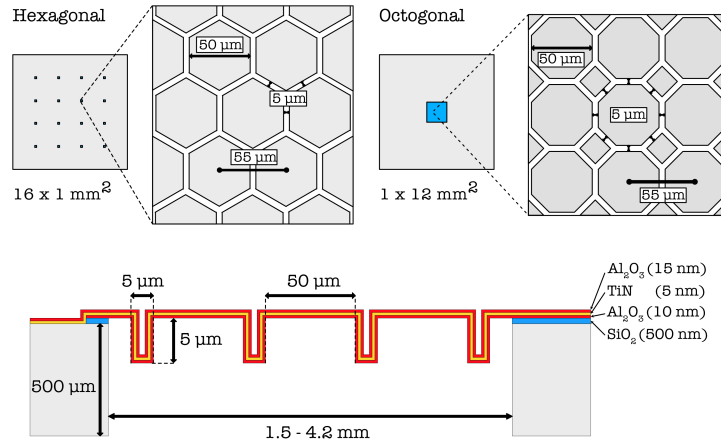


**Figure 4:** The metamaterials are suspended within a silicon frame with a dimension of 20 mm by 20 mm. For the hexagonal pattern, 16 windows with a surface of approximately 1 mm<sup>2</sup> are opened in which the metamaterial film is suspended. For the octagonal pattern, the film is suspended in a single window with a surface of approximately 12 mm<sup>2</sup>

With this rule in mind, the second pattern is an octagonal pattern which is designed to work in conjunction with a TimePix chip. First, the square lattice of the pattern matches the pitch/displacement of the pixel pads on a TimePix chip. Second, the octagonal-shaped domes have a focusing effect on SEs, which guide the SEs from each tynode in a 'channel' above the individual pixel pads. This effect is also needed to focus the SEs onto the collection surface of the pixels, which has a smaller dimension than the spacing of a pixel.

The focusing effect of these octagonal-shaped cells have been simulated with COMSOL (figure 3). A cell with a height of 5 μm is already sufficient to focus SEs, but the focusing point can be tailored by varying the height of the unit cells. The simulation also shows that PEs and SEs that enter the small square pattern in the corner of each octagonal are 'lost', since they land next to the pixel pads. This needs to be taken into consideration when estimating the collection efficiency.

The dimensions of the cells are chosen to match the pitch of the pixels and is shown in figure 4 for both patterns. The rib height and width are 5 μm, which is relatively shallow. Incoming electrons can still reach the bottom of the rib and contribute to electron multiplication. Increasing the height further, the chance for incoming electrons to reach the bottom of the trench will decrease, since only electrons that enter perpendicularly will manage to do so. The unit diameter is 50 μm and has a pitch of 55 μm (which is the same as the pitch between pixels). The windows are differently sized and are designed to open arrays with 16x16 or 64x64 unit cells. An additional margin is added to account for the slope due to the etching process. The windows have a width of (0.88+0.74) mm and (3.52+0.74) mm with a surface area of 2.64 and 18.2 mm<sup>2</sup>, respectively.

The emission film is a tri-layer Al<sub>2</sub>O<sub>3</sub> composite with a thickness of 10/5/15 nm. This film is functionalized as a SEE membrane by encapsulating a TiN layer, which is needed to sustain electron emission for prolonged operation [6].

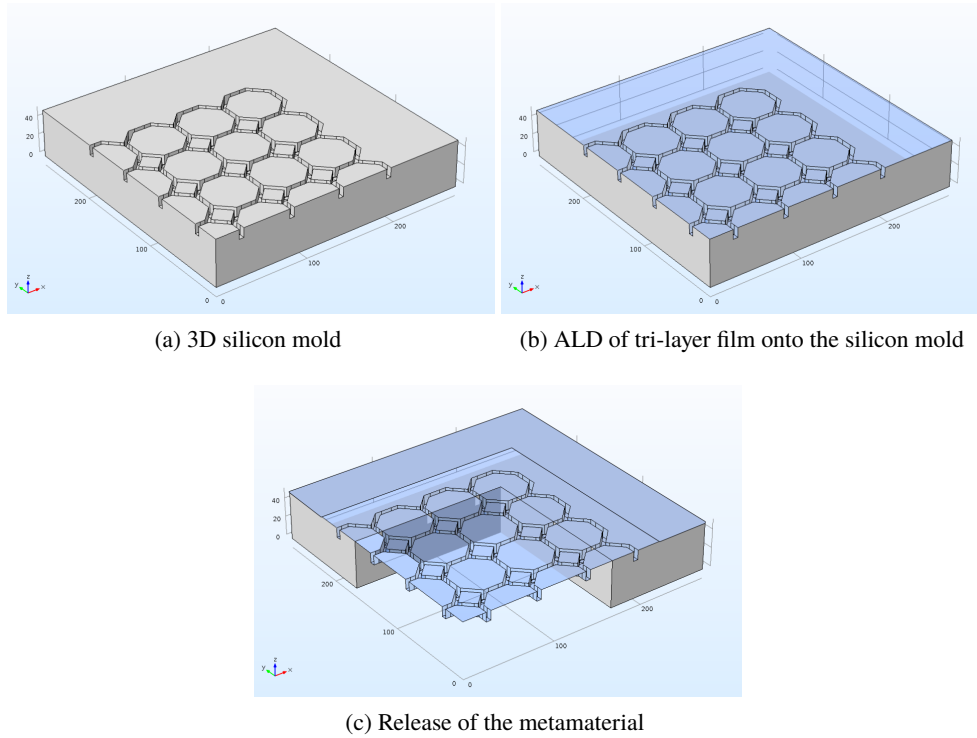


**Figure 5:** Flow chart

### 3 Fabrication

a 4-inch p-type ( $5\text{--}10\ \Omega\ \text{cm}$ ) wafer with a thickness of  $500 \pm 15\ \mu\text{m}$  is used as substrate. The wafers are cleaned with a standard cleaning procedure before a zeroth layer is added with markers for contact alignment. The sequence of the cleaning procedure is as follows: a plasma oxygen etch, a HNO 100% bath for 10 min, a demineralized water rinse for 5 min, a HNO 65% bath at  $110\ ^\circ\text{C}$  for 10 min and another water rinse.

The process can be divided in three parts. In the first part, a 3D mold is etched within the silicon substrate (figure 5a). A  $3\text{-}\mu\text{m}$ -thick photoresist (PR) layer is used as a masking layer for a deep-reactive-ion-etch (DRIE) in a Rapier Omega i2L DRIE etcher. The hexagon pattern is transferred to the PR and trenches with a depth of  $5\ \mu\text{m}$  are etched into the silicon substrate. The wafers are then cleaned with oxygen plasma to remove residual polymers from the DRIE process followed by a standard cleaning procedure. Afterwards, the wafers are put in an oven at  $1100\ ^\circ\text{C}$  to wet thermally grow a silicon dioxide layer with a thickness of  $500\ \text{nm}$ . This layer will act as a sacrificial and stopping layer.

In the second part, the tri-layer film material is deposited conformally on the mold (figure 5b). First, a layer of  $\text{Al}_2\text{O}_3$  is deposited by atomic-layer-deposition (ALD) in a thermal ALD ASM F-120 reactor at  $300\ ^\circ\text{C}$  using trimethyl-aluminum (TMA) and water as a precursor and reactant, respectively. A strip of the newly deposited layer is removed from the edge of each die to create a contact point for the next layer to the silicon substrate. First, the  $\text{Al}_2\text{O}_3$  layer is plasma etched in an Omega Trikon plasma etcher. Then, the silicon dioxide layer is removed with a plasma etch



in a Drytek plasma etcher. The wafers are cleaned afterwards using a new procedure omitting the 'fuming' HNO 65% bath. Next, a layer of ALD titanium nitride is deposited in an Ultratech Fiji G2 using titanium chloride ( $\text{TiCl}_4$ ) as precursor and nitrogen plasma as reactant at 250 °C. The third layer of  $\text{Al}_2\text{O}_3$  is then deposited with the same recipe as the first layer in the same reactor.

In the third part, the metamaterial will be released by opening windows in the silicon substrate (figure 5c). First, a plasma-enhanced chemical vapor deposition (PECVD) oxide layer with a thickness of 1  $\mu\text{m}$  is deposited on the front side of the wafer in a Novellus Concept One system. This oxide layer protects the tri-layer film from subsequent etching steps. The backside of the wafer is stripped by using two plasma etches. The ALD TiN and ALD  $\text{Al}_2\text{O}_3$  layers are stripped in the Omega Trikon plasma etcher, while the thermal oxide is removed in the Drytek plasma etcher. Once, the backside is stripped and cleaned, a PECVD oxide layer with a thickness of 5  $\mu\text{m}$  is deposited on the backside of the wafer in the Novellus Concept One system. This PECVD oxide layer is the masking layer for DRIE. The pattern of the window openings and scribe lines are transferred using PR with a thickness of 3.1  $\mu\text{m}$ . This pattern is etched into the PECVD oxide masking layer in the Drytek plasma etcher. The wafers are now ready for the final release using the Rapier Omega i2L DRIE etcher. First, a fast DRIE recipe is used to etch a depth of approximately 495  $\mu\text{m}$  into the silicon substrate until the rib pattern of the metamaterial become visible. The protective PECVD oxide on the front side is then removed in a HF vapor etch chamber using 4 etching cycles of HF and ethanol with a flow of 190 sccm and 220 sccm, respectively, for a duration of 10 min per cycle. If this oxide layer is not removed before the final release steps, it will be the main contributor to the stress within the film and can cause ruptures. Afterwards, the wafer is cleaved along the scribe lines. The individual dies are transferred to a carrier wafer with pockets to hold them. The remaining 5  $\mu\text{m}$  of silicon are removed with a slower DRIE recipe within the Rapier. The dies are then cleaned with oxygen plasma in a TEPLA plasma cleaner to any remove residual polymers (from the DRIE process). The final release is the removal of the thermal oxide layer, which is again performed in a HF vapor etch chamber using the same recipe as above.

## 4 Experimental setup

### 4.1 Transmission secondary electron yield

The transmission secondary electron yield is measured with a collector-based method within a scanning electron microscope (SEM) as shown in figure 6a. A more thorough description of the method is given in ref [6]. First the electron beam current is measured within a small Faraday cup next to the sample. The beam is then moved to the window in the sample in which the ultra-thin film is suspended. During the measurement, the beam is scanned over the surface in a zigzag pattern using the image acquisition mode of the SEM. This mode lowers the electron dose per unit surface, which mitigates charge-up effects and/or the built-up of surface contamination. The sample holder, mesh grid and collector are connected to Keithley 2450 source meters via a feedthrough into the vacuum chamber. The transmission current is measured directly within the collector, while the reflection current is determined indirectly using the sample current. The sample is either negatively biased at  $-50\text{ V}$  or positively at  $+50\text{ V}$ . The former setting is used to determine the total reflection and transmission yield, while the latter is used to measure the back- and forward scattered electrons.



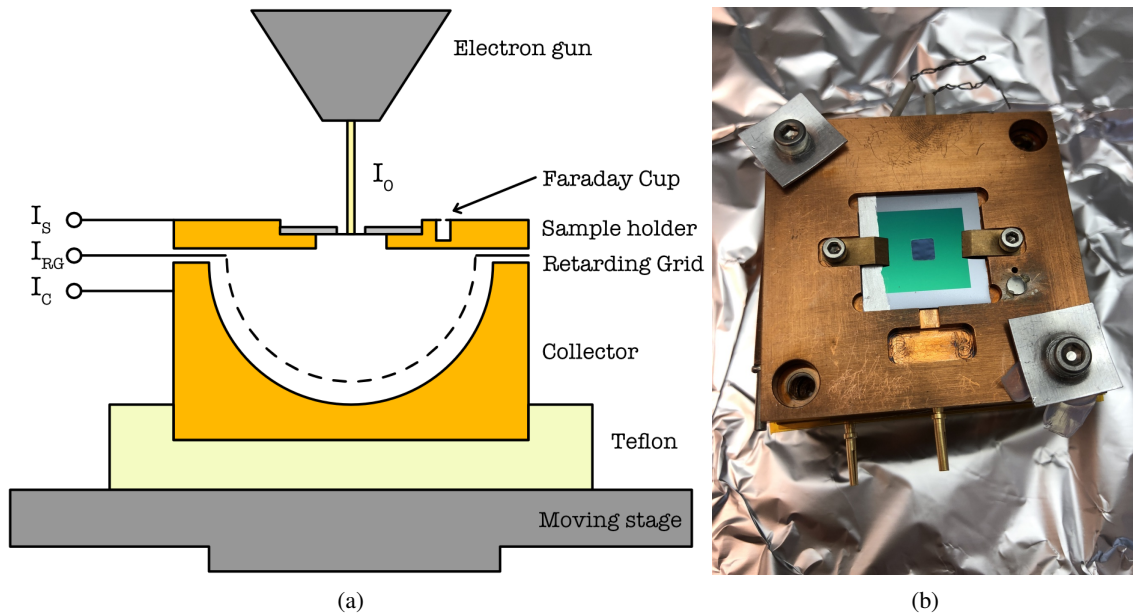


**Figure 6:** Experimental setup. (a) schematic drawing of the collector. (b) The copper collector with one of the octagonal metamaterial film mounted in the sample holder.

By subtracting the results, the 'true' reflection and transmission secondary electron yields can be found. The PE energy range from 0.3 to 10 keV with a beam current of 0.06 to 0.54 nA. The current depends on the PE energy and is measured for each energy. The following SEM settings are used during the measurement: a dwell time of 1  $\mu$ s, a magnification of 50X, a Half-full-window (HFW) of 2.56 mm and a resolution of 1024 x 884. Using these settings, the area of the irradiated surface can be estimated, which in this case is 5.66 mm<sup>2</sup>. The obtained yields are averaged over the surface and over time, i.e. the yield is calculated from multiple frames.

## 4.2 Surface scan & Yield maps

A transmission secondary electron yield map, as a function of the coordinates of the surface of the membrane, can be obtained during a (single) SEM image acquisition. A yield map will show the difference in electron emission across the surface. The method is described in appendix A and operates on the same principles as SEM image construction. The SEM settings are chosen such that the Keithley 2450 sourcemeters are able to map the measured current (as of function of time) to the pixels in the SEM image. This method requires a much slower scan speed compared to the method presented in section 4.1. Also, only one image frame is acquired. A dwell time of 1 ms is chosen, which is a compromise between speed and accuracy. A larger dwell time might cause charge-up effects and/or surface contamination. The resolution of the image is 512 x 442 acquired with a dwell-, line- and frame time of 1 ms, 560 ms and 4.2 min respectively. The electron beam energy used to acquire the image is 3.2 keV with a current of 0.29 nA, which have the highest transmission yield for the membranes considered in this paper. The magnification is 500X or 1000X, which shows the difference in yield across the 3D structure of the metamaterial more clearly.

## 5 Results & discussion

### 5.1 Fabrication

SEM images of the front- and backside of a metamaterial film with a hexagonal pattern is shown (figure 7). The contrast in the image is due to the 3D structure of the film. In figure 7a, the ribs extrude into the plane and behaves as 'trenches' from which it is more difficult for SEs to escape. Therefore they appear darker. In figure 7b, the backside of the film is shown. In this case the ribs protrude out of plane and appear brighter. The 3D structure of the film is more apparent in figure 8, which shows a curled up film showing both sides. In figure 8, SEM images of the metamaterial with the octagonal pattern is shown. The black dots on the surface are residues from the fabrication process. On a different sample, a close-up of a broken film shows flakey residues on the film and the ribs (figure 10). These are residues of the HF vapor etch. Also, in figure 10b, the etch line of the DRIE process is indented in the ribs. The DRIE process is a cyclic process of etching and passivation. For the samples in this paper, 8 cycles were used to etch 5.1  $\mu\text{m}$  into the silicon wafer.

There are two critical steps in the fabrication process of these metamaterial films. First, the second and third DRIE process, used to open the windows from the backside of the wafer, require careful monitoring. Although, the thermal oxide layer act as a landing layer, the etch rate is different for windows with different widths. In general, more open features are etched faster. As such, there is a chance of over etching, which can damage the ribs of the metamaterial film. Second, after the final release step in the HF vapor chamber, the metamaterial films are fragile. They are prone to breakage due to air pressure differences and/or electrostatic forces.

### 5.2 Transmission secondary electron yield

The metamaterial films have been measured with the unit cells/domes facing up- and downwards. Upward facing will have a more uniform response, since the emission surface is flat. Downward facing will have the focusing effect. Depending on the application, one might be more preferred than the other.

The maximum transmission yield of the octagon pattern with a window size of 12.4  $\text{mm}^2$  is 2.15(3.15 keV). Placed upside down, 1.85(3.15 keV). Critical energy of approximately 1.1 keV. The difference in yield when the sample is placed facing up or down can be explained by either (1) the difference in thickness of the alumina layer or (2) the difference due to the metamaterial layout. Especially the ribs can give a different yield. PE entering a trench, can generate SEs in an open space (hexagon units), while when turned upside down, the SEs are generated within the narrow rib. SEs can be recaptured and the electric field within the rib is weak. The maximum transmission yield of the hexagon pattern with a window size of 1  $\text{mm}^2$  is 1.7(3.05 keV). Placed upside down 1.85(3.05 keV). The lower yield of the hexagon is due to the window size, which recapture some of the emitted electrons and lowers the yield. The octagon sample has an almost open field of view. The effect is also clearly shown in the reflection yield, when the window is facing upwards. The reflection yield is much lower.

Compared to the bi-layer films in [5], which had similar thickness: 2.1(2.55 keV) with a critical energy of 1 keV. Compared to the tri-layer films in [5]: 2.7(2.75 keV)

The membranes presented here are slightly thicker in comparison with the flat films. The slight shift in critical energy  $E_c$  of 150 eV and also the max peak of 400 – 600 eV indicates it.

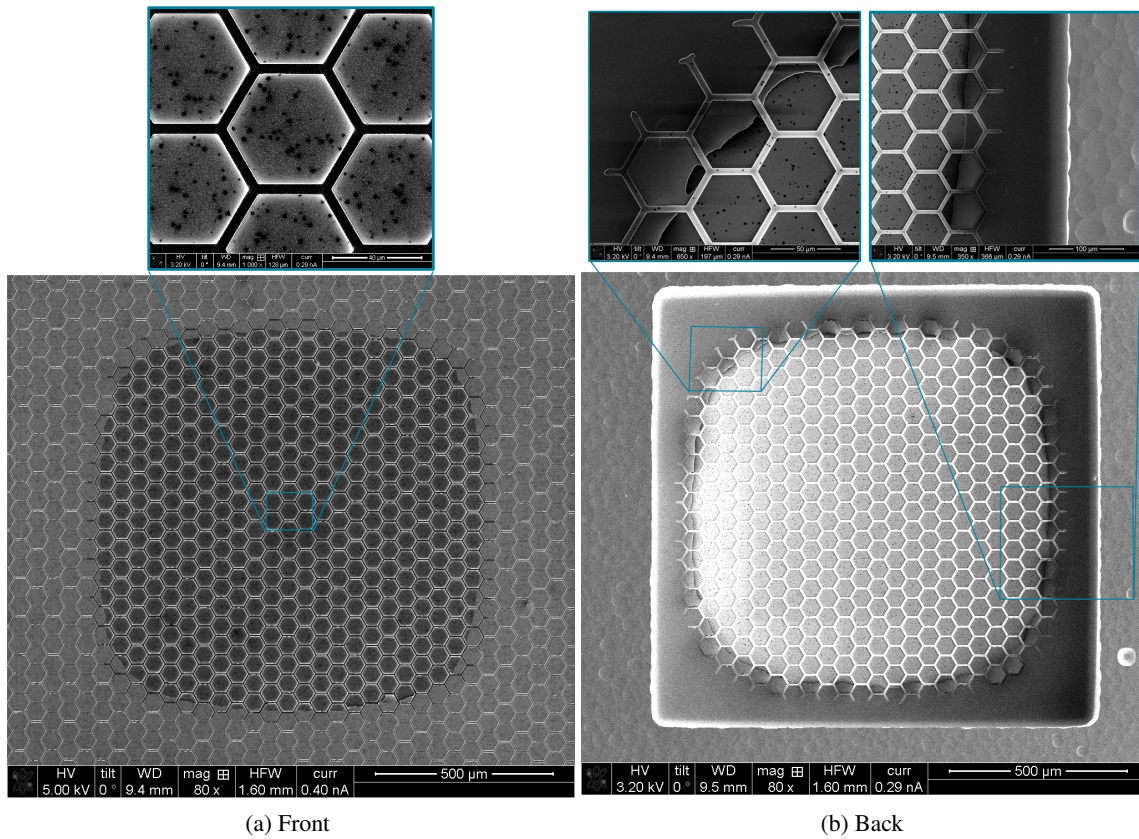


**Figure 7:** SEM images of a metamaterial film with a hexagonal pattern. (a) The contrast between the active area and the window frame is due to the transparency of the film for 5 keV electrons. (b) On the backside, the ribs protrude outwards and appear brighter since SEs are generated closer towards the SE detector of the SEM. On the edge, the ribs disappear into the silicon substrate.

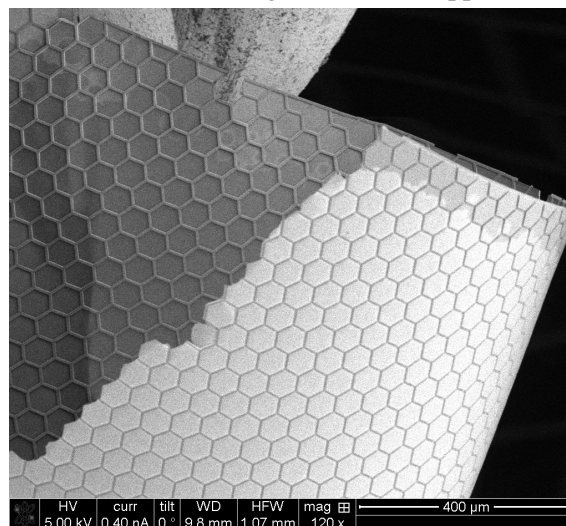


**Figure 8:** A SEM image of a broken film curled up after release. It clearly shows the ribs of the honeycombs on the front- and backside.



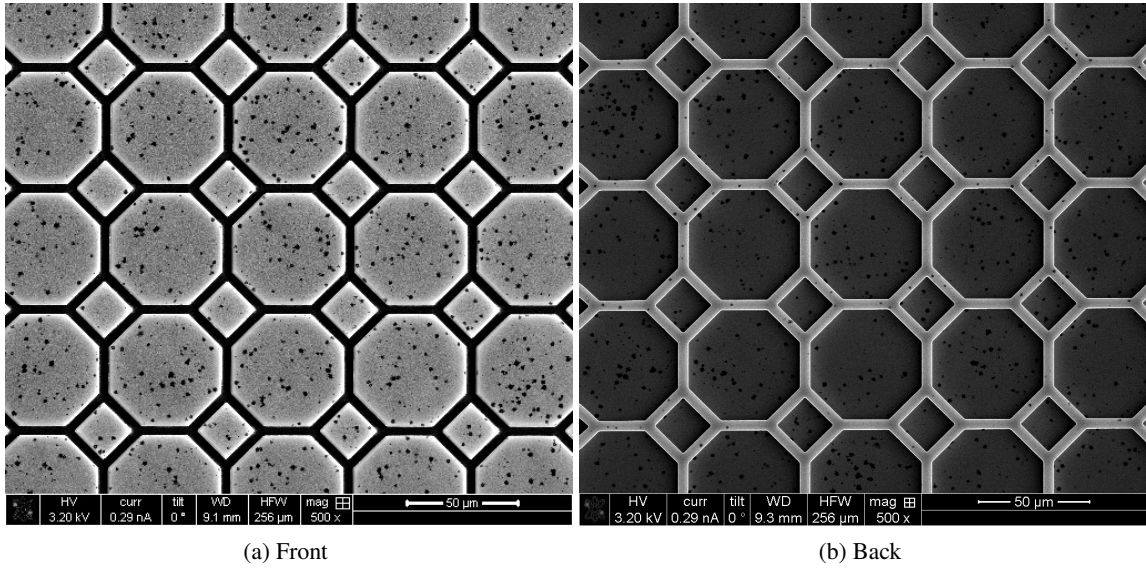


**Figure 9:** SEM images of a metamaterial film with an octagonal pattern.

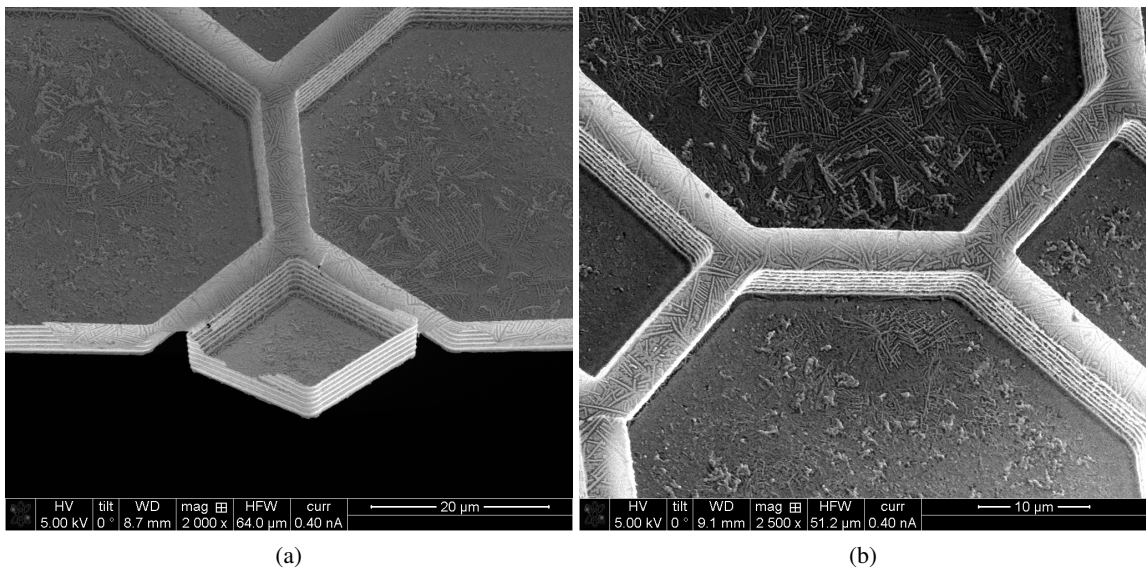


**Figure 10:** SEM images of a broken metamaterial film with an octagonal pattern. The etch lines of the DRIE process is visible on the ribs. (a)

The difference in thickness can stem from either: (1) production parameters or (2) residues from processing (black dots on the surface/ crystals on the surface). The transmission yield is comparable to the bi-layer, but lower than the tri-layer.

### 5.3 Active surface & Collection efficiency

The active surface of a tynode can be determined by measuring transmission yield as function of the coordinates of a tynode. In 13, the response of an octagon tynode is shown. The yield response

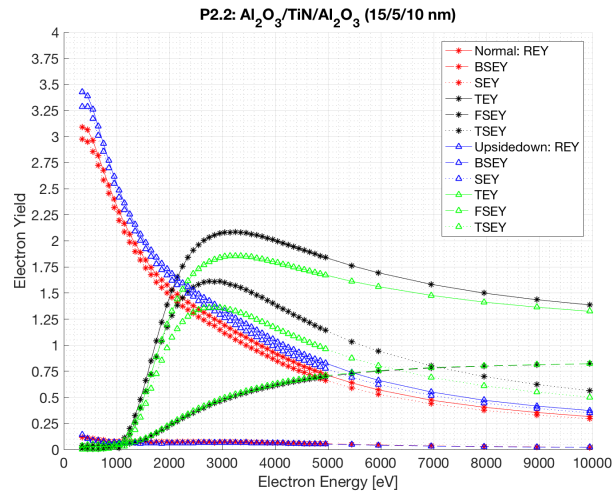


**Figure 11:** Electron yield curves of a hexagonal metamaterial film with a thickness of 15/5/10 nm

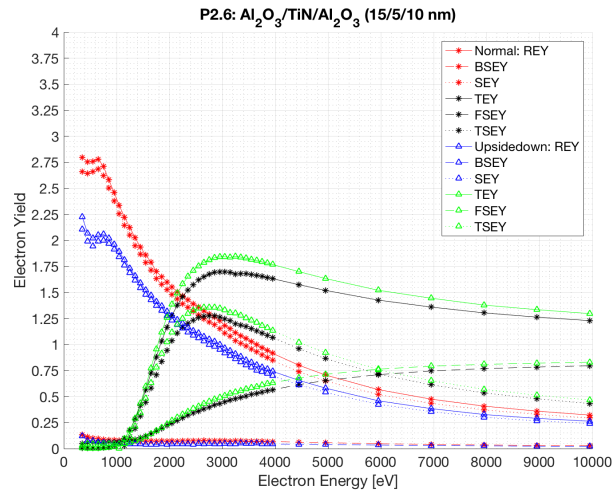


**Figure 12:** Electron yield curves of an octagonal metamaterial film with a thickness of 15/5/10 nm

is higher than one on the entire surface, thus we can assume that the active area is 100%. The variation of the yield across the surface is due to the vertical walls, which has a higher transmission yield response due to the entry angle into the film. It has been shown that more SEs are generated for PEs that enters an angle. When placed upside down, the situation is slightly different. There is no focusing effect (except within the ribs). The response will also be different and a more uniform emission is expected, since the emission surface is mostly flat. Within the ribs, the transmission yield is lower due to recapture of SEs in the rib with a 1:1 height/width ratio.

It is difficult to predict what the collection efficiency is of the honeycomb pattern. The yield map shows that it has a 100% active surface area. However, the hexagon pattern does not match the square pitch of the pixel chip. Using a planar anode, it can be potentially 100%. yield map showed that the metamaterial has a 100% active surface with higher transmission yield near the vertical walls of the hollow ribs. Depending on the read-out, this means a collection efficiency of 100%

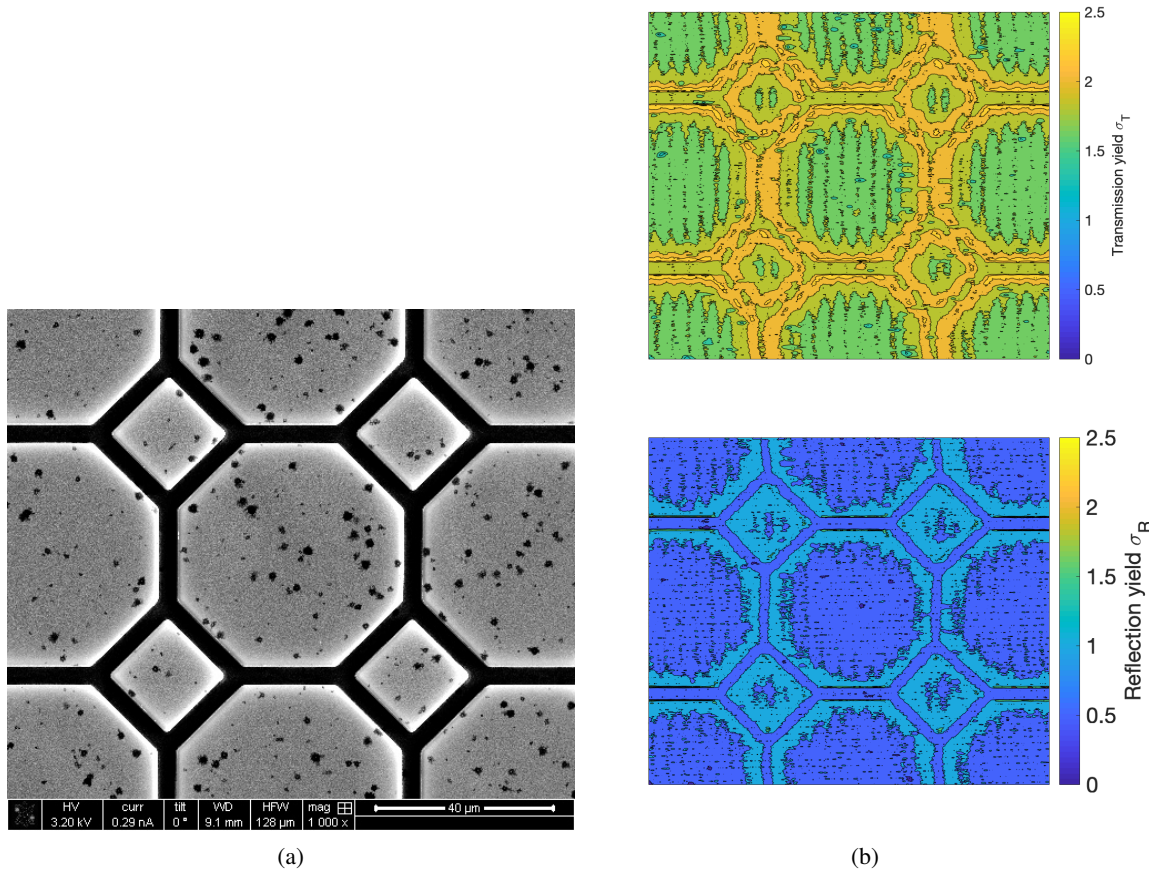


**Figure 13:** Yield map of octagon tynode with ribs facing downwards. The reflection yield map matches the SEM image. The former is determined from the sample current, while the latter is determined from SE emission from the sample. The glow near the edge of the octagon/square is visible on both pictures. The transmission yield near the vertical walls is higher due to the angle of incidence of the PEs.

when for instance a planar anode is used. For TiPC, the collection efficiency would be defined as the number of photoelectrons emitted from the photocathode can trigger a signal in a pixel. In this case, the focusing of the octa pattern can direct most electrons to the pixel pad when they are emitted from the octagon. Using the pattern presented here, the collection efficiency would be the surface of the octagon divided by a pixel surface. The collection efficiency is then just 68%. If we assume the SEs generated within the ribs ends contributes as well, then it is 82%. The remaining 18% are the squares in the pattern, which will form a channel on their own which ends next to the pixel pads. A solution is to use a different pattern for the first tynode. For instance, a simple square pattern. This pattern is less strong. A solution to guarantee that electrons in the ribs are collected as well is to use a different shape, such as a U- or V-shaped beams. This can be achieved by using different recipes in DRIE or using wet chemical etching using KOH, which is anisotropic.

The largest metamaterial membrane that were made has a surface of approx.  $12.4 \text{ mm}^2$ . This



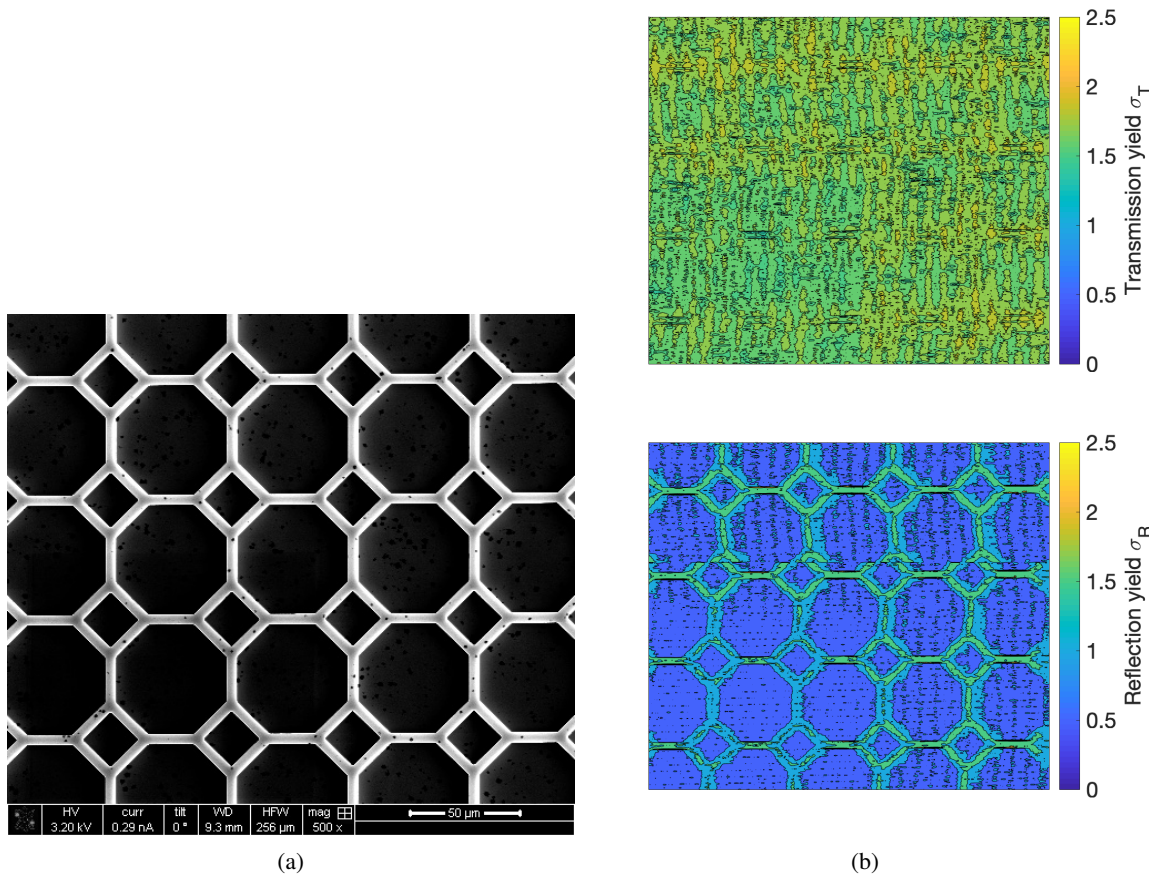


**Figure 14:** Yield map of octagon tynode with ribs facing upwards. The transmission yield map is more homogeneous. In reflection, the vertical walls of the ribs generate a lot more Reflection SEs due to the angle of incidence of the PEs.

is much larger than achievable with a flat membrane. Though, this is almost at the limit. The films are prone to breaking due to electrostatic attraction, deformation by pressure differences and, in one case, by simply looking at it. The window surface is designed to cover 64x64 pixels. One can sacrifice a few rows of pixels to create a silicon frame with smaller windows. For instance, 30x30 pixels windows and a frame with 4 pixels width (0.22 mm)

## 6 Conclusion & Outlook

Mechanical metamaterials can be functionalized as transmission dynodes by using a tri-layer  $\text{Al}_2\text{O}_3/\text{TiN}/\text{Al}_2\text{O}_3$  film deposited by atomic-layer-deposition. The 3D structure of the metamaterial allows films to have an extreme surface/thickness ratio in comparison with flat membrane. Meta-material can have a 100% active surface over a large-surface. The largest surface area was approximately 12.4 mm<sup>2</sup> with a thickness of 10/5/15 nm for a tri-layer  $\text{Al}_2\text{O}_3/\text{TiN}/\text{Al}_2\text{O}_3$  film. The transmission yield response of the metamaterial with is measured by determining the yield map. Although there are some variations in transmission yield across the surface, transmission secondary



electron emission is measured. The metamaterial has been successfully functionalized by using a tri-layer film. In addition, the hexagon/octagon cells can be operated in focusing mode by facing the cell towards the next target cell. Facing upside down gives a more uniform response. (COMSOL).

The thickness needs to be reduced to improve the transmission electron emission performance. This can be achieved by either improving the final release steps by improving the selectivity of the DRIE recipe towards Si and Al<sub>2</sub>O<sub>3</sub>. Or, a different road is to create a silicon frame in which the thinner metamaterial is suspended. The open surface would be intersected by a few silicon beams. By sacrificing a few rows of pixels, the silicon frame can provide additional strength. The collection efficiency of the tynodes can be further improved by using U- or V-shaped ribs. SEs generated within a rib would then be extracted in either side of the rib. Other patterns can be designed for the first tynode, which can collect more PEs towards a tynode "channel". And furthermore, the TSEE of the metamaterial can be increased by using different ALD materials, such as MgO.

## References

- [1] H. van der Graaf, H. Akhtar, N. Budko, H. W. Chan, C. W. Hagen, C. C. Hansson, G. Nützel, S. D. Pinto, V. Prodanović, B. Raftari, P. M. Sarro, J. Sinsheimer, J. Smedley, S. Tao, A. M. Theulings, and K. Vuik, "The Tynode: A new vacuum electron multiplier," *Nuclear Instruments and Methods in Physics Research, Section A: Accelerators, Spectrometers, Detectors and Associated Equipment*, vol. 847, no. June 2016, pp. 148–161, 2017.
- [2] T. Hakamata, Ed., *Photomultiplier tubes*, 3rd ed. Hamamatsu Photonics K.K., 2007.
- [3] S. X. Tao, H. W. Chan, and H. Van Der Graaf, "Secondary electron emission materials for transmission dynodes in novel photomultipliers: A review," *Materials*, vol. 9, no. 12, 2016.
- [4] M. Hagino, S. Yoshizaki, M. Kinoshita, and R. Nishida, "Caesium Activated CsI Transmission-type Secondary Emission Dynode," *Advances in Electronics and Electron Physics*, 1972.
- [5] V. Prodanović, H. W. Chan, H. V. Graaf, and P. M. Sarro, "Ultra-thin alumina and silicon nitride MEMS fabricated membranes for the electron multiplication," *Nanotechnology*, vol. 29, no. 15, 2018.
- [6] H. Chan, V. Prodanović, A. Theulings, C. Hagen, P. Sarro, and H. v.d. Graaf, "Secondary Electron Emission from Multi-layered TiN/Al<sub>2</sub>O<sub>3</sub> Transmission dynodes," *Arxiv preprint*, vol. -, no. -, pp. -, 2020.
- [7] V. Prodanović, "Ultra-thin mems fabricated tynodes for electron multiplication," Ph.D. dissertation, Delft University of Technology, 2019.
- [8] K. Davami, L. Zhao, E. Lu, J. Cortes, C. Lin, D. E. Lilley, P. K. Purohit, and I. Bargatin, "Ultralight shape-recovering plate mechanical metamaterials," *Nature Communications*, vol. 6, p. 10019, 2015.

## A Secondary electron yield map

A SEM image is constructed by measuring the SE emission from a specimen, while an electron beam is scanned over its surface in a zigzag pattern. The speed of a scan is determined by the dwell time, the time the electron beam irradiate on a surface corresponding with a pixel in a SEM image. The line time is the time to acquire one row of the image, which is the number of pixels in the row

+ additional time to reposition the beam onto the front of the next row. The frame time is the time to acquire the entire image. The resolution is the number of pixels.

The transmission yield as a function of the coordinate of a SEM image can be obtained by measuring the transmission current during image acquisition. The background current is measured before the start, while the E-beam is blocked. Image acquisition starts, while the sample, grid and collector currents are measured simultaneously. After acquisition is done, the E-beam is blocked again. The background current is measured again. The settings are choosing as follow: dwelltime 1 ms, Resolution: 512 x 442, linetime 560 ms, frametime: 4.2 min.

The yield map reconstruction is performed with the same principle as the image reconstruction. The current is registered as a function of time. The background current is determined by the first and lasts few seconds. The rest of the currents are cut into 540 ms sections and rearranged in a 2D matrix. Each line is then matched to the corresponding line in the SEM image.

There are some artefacts. The image can be shifted due to the position of the cut. A timing delay can create artefacts in the image. There is a delay in either the SEM or the Keithley in which an extra pause is detected. The image is then distorted. These glitches need to be removed manually. A line consists of 540 ms, while there is only 512 pixels in a row. The 540 pixels can be shifted left and right to match the SEM image. A measurement point in Keithley can be acquired with a maximum rate of  $333\text{ s}^{-1}$  or 3.3 ms per data point. The data point is mapped to the closest pixel. The open pixels are calculated by averaging over the neighboring pixels.

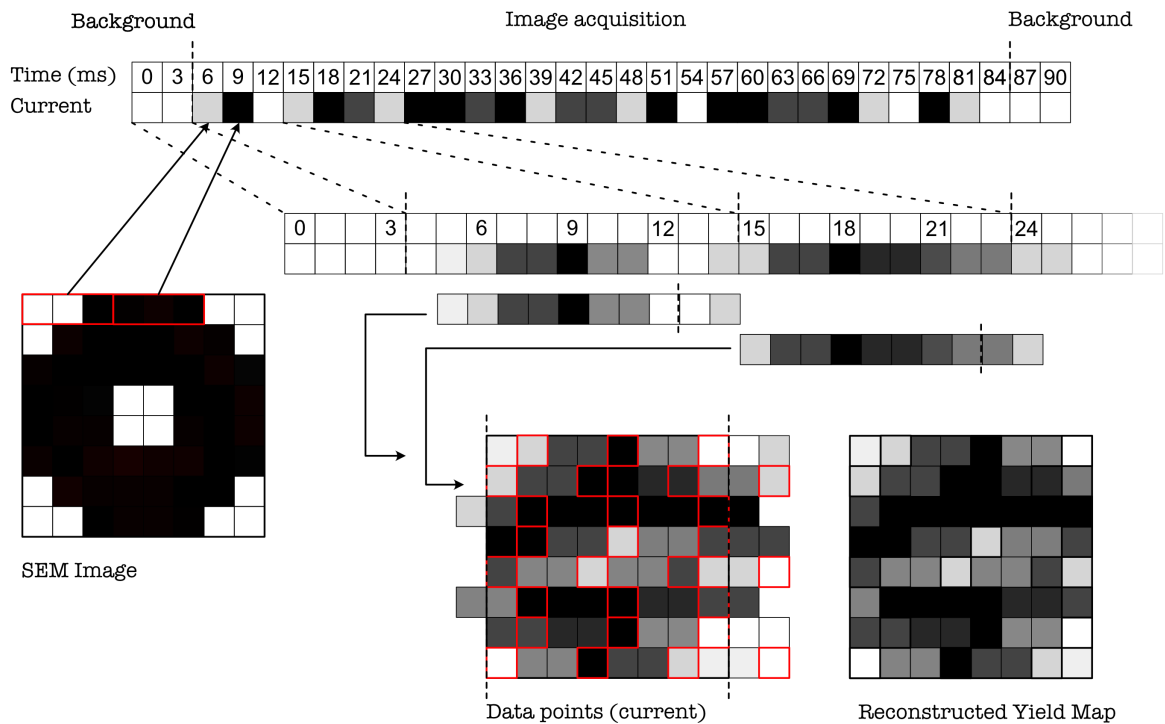


**Figure 15:** text